PIER M

Compact Broadband Low-Pass Filter with Novel Fishbone Structure Based on Spoof Surface Plasmon Polariton

Haodong Xu[1,2], Fushun Nian[1,2,*], Jianqin Deng[2], and Muzhi Gao[3]

[1] *School of Instrument and Electronics, North University of China, Taiyuan 030051, China*
[2] *Technology on Electronic Test & Measurement Laboratory, Qingdao 266555, China*
[3] *School of Control Science and Engineering, China University of Petroleum (East China), Qingdao 266555, China*

ABSTRACT: A compact spoof surface plasmon polariton (SSPP) low-pass filter is proposed. By adopting a novel fishbone structure, the effective depth of the groove is increased, reducing the filter width by 24.84%. The length of the filter is reduced by 22.23% with a new transmission structure. To intuitively display this structure, the filter is designed and fabricated. The area of the filter is 47.44 mm × 8 mm. The results demonstrate that the insertion and return losses are less than 3 dB and greater than 13 dB, respectively, in a wideband range of 0–10.00 GHz

1. INTRODUCTION

As surface (electromagnetic) waves, when surface plasmon polaritons (SPPs) are excited by the resonant interactions between the surface electrons of metals and the electromagnetic field of light, they propagate along the metal-dielectric interface [1]. Under the necessary condition that the metals and dielectrics have opposite permittivity, the properties of the SPPs can be customized by altering the surface structure of the metals. SPPs exhibit unique optical properties and have been extensively studied in different optical bands. Plasmonic materials are popular research directions, such as graphene [2–4], Bi_2Se_3 [5], Dirac semimetals [6], topological chiral materials [7], nodal-line semimetals [8], and Weyl semimetals [9]. In addition, the applications of plasmons and their materials in photodetection [8, 10 11], catalysis [8, 12], and desalination [8] have also attracted a lot of thermal research.

Previous reports [13] indicate that metals can be considered perfect electrical conductor (PEC) in the terahertz, microwave, and millimeter wave frequency bands; in these bands metals and dielectrics do not have opposite permittivity, resulting in SPPs that cannot be excited [14]. Therefore, the concept of spoof surface plasmon polariton (SSPP) was proposed by J. B. Pendry et al. [22, 15]. By creating periodic grooves or hole arrays on metals, SSPP can be excited in the terahertz and lower frequency bands, enabling the application of SSPP in frequency bands below the optical band [16]. The structures of SSPP based on this theory have been extensively investigated in recent years [17–24].

Nevertheless, in previous studies, the structures were all 3-D structures, and due to their bulk size, they cannot adapt to the development trend of circuit integration and miniaturization. This limitation restricts the application of SSPP in integrated circuits. Consequently, many studies have focused on developing miniaturized SSPP structures [25–29]. Ma et al.

proposed an ultrathin and flexible conformal surface plasmon structure [30]. They later introduced a planar metal ultrathin metamaterial [31, 32]. These studies significantly advanced the application of SSPP in the terahertz, microwave, and millimeter waves frequency bands. However, despite these efforts, the size of various SSPP structure filters can be optimized further for miniaturization and integration.

In this paper, a compact low-pass filter with a novel fishbone structure based on SSPP is proposed within a passband range of DC∼10.00 GHz. The proposed structure achieves a similar bandwidth and better filtering performance than previous structures, and the size of the SSPP filter is significantly reduced. First, an SSPP cell was designed, and its dispersion characteristics were simulated to understand the relationship between its parameters and asymptotic frequencies. Subsequently, a complete SSPP filter structure was designed by combining six identical SSPP cells. The optimal design for the SSPP low-pass filter was determined by analyzing the impact of key parameters through simulations and optimizing the S-parameters for the full structure filter. Finally, the compact SSPP low-pass filter was fabricated and assessed. The measurement results demonstrate that the insertion loss (IL) is less than 3 dB, and the return loss (RL) is greater than 13 dB in a wideband range of 0–10.26 GHz. The proposed filter can be used to compose microwave circuits, such as mixer, multiplier, and comb generator. In addition, the passband of the proposed filter can also be easily customized by changing some specific parameters.

2. DESIGN OF THE SSPP FILTER

2.1. Dispersion Characteristic of the SSPP Cell

The proposed SSPP low-pass filter has a novel fishbone structure. The SSPP cell includes a structure loaded at both ends of a microstrip, which resembles a sloping limb with several transverse branches in a step pattern with gradually deceasing

* Corresponding author: Fushun Nian (nfswxmnk825@163.com).
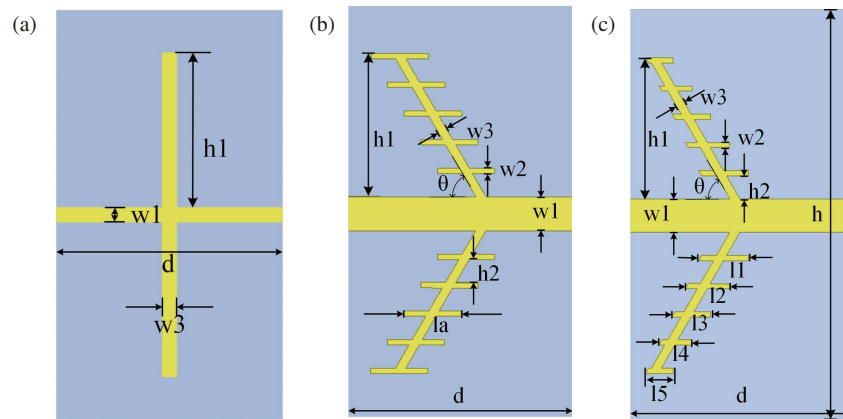
FIGURE 1. Schematic diagram of the SSPP unit cell structure: (a) Cell A, traditional structure, (b) Cell B, with long transverse branches and (c) Cell C, with short transverse branches.
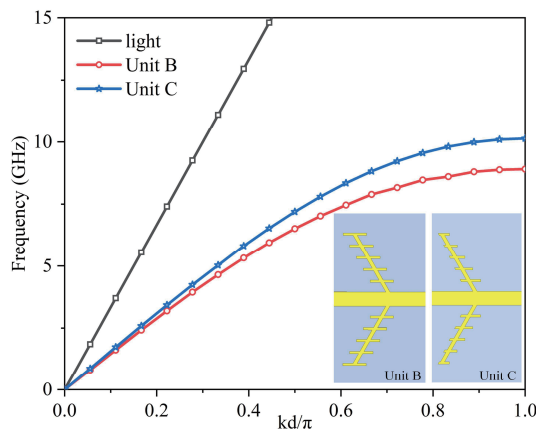
FIGURE 2. Dispersion diagrams for light, Cell B and Cell C.
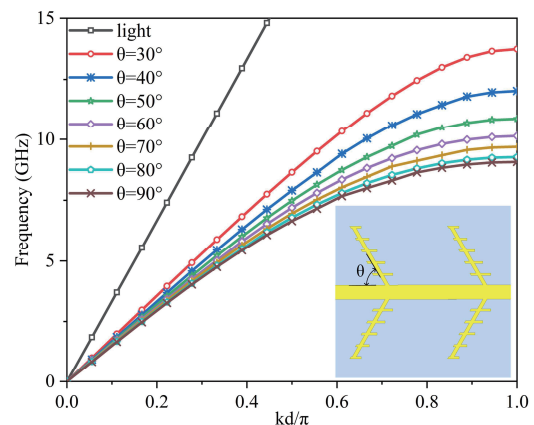
FIGURE 3. Relationship between the asymptotic frequency of the SSPP filter cell and angle θ.

length. Fig. 1(c) illustrates the SSPP unit cell structure. The dielectric substrate is F4B with a dielectric constant $\varepsilon_r = 2.65$ and a thickness of 0.5 mm. A copper microstrip and layer that are 0.035 mm thick are used on the upper and lower surfaces of the substrate, respectively.

Figure 1(b) shows the SSPP unit cell (Cell B), which includes transverse branches on sloping limbs that are symmetrically distributed on both sides of the microstrip. The limbs at symmetrical positions form an angle $\theta = 60°$ with the microstrip. The lengths of the horizontal branches on the sloping limbs gradually decrease from the bottom to the top of the structure, as shown in the final cell structure (Cell C, as shown in Fig. 1(c)). The binding of the filter structure to the electromagnetic field is enhanced by adding transverse branches. At the same time, the design freedom is also increased, and the performance of the filter is more fine-tuned. For reference, the main parameter values are provided in Table 1.

The dispersion curve is an important attribute of SSPP cells. The relationship between the frequency f and the inherent phase shift φ can be written as:

$$f = \frac{ck_x}{2\pi} = \frac{c}{2d} \cdot \frac{kd}{\pi} = \frac{c}{2d} \cdot \frac{\varphi}{180} \qquad (1)$$

where d, k_x, and c are the periodic distance in the periodic structure, the propagation constant, and the speed of light in vacuum, respectively. $c/2d$ represents the slope of the dispersion curve, and kd/π represents a normalization of the inherent phase shift φ. This formula is used to generate the dispersion curves.

The eigenmode solver in HFSS was used to design the above SSPP structure cells, and their dispersion curves were simulated, as depicted in Fig. 2. Notably, when the horizontal branches were the long branches shown in cell B, the asymptotic frequency of the SSPP filter cell was 8.9 GHz. However, the asymptotic frequency increased to 10.2 GHz when the lengths of the horizontal branches on the sloping limbs in cell C were decreased. The results indicate that when the transverse length of SSPP cell B is shortened to cell C, the equivalent capacitance becomes smaller, and the asymptotic frequency increases slightly. However, compared to the traditional SSPP structure (cell A), the groove depth $h1$ of the proposed structure (cell C) can also be reduced by 26.22% [31].

Since other parameters have no obvious influence on the filter performance, only the influence of angle θ, periodic distance d, and other main parameters on the filter performance is discussed.
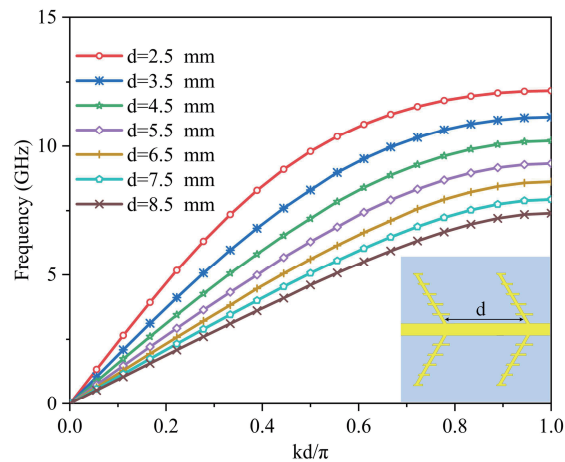
FIGURE 4. Relationship between the asymptotic frequency of the SSPP filter cell and the periodic distance d in mm.
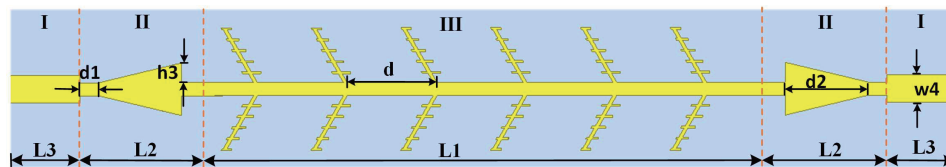
FIGURE 5. Full structure of the designed SSPP low-pass filter.

To investigate the relationship between angle θ and the asymptotic frequency of the SSPP filter cell, the dispersion curves for several different θ values were simulated. As depicted in Fig. 3, when the value of θ was varied from $30°$ to $60°$ and then to $90°$, without altering any other parameters, the asymptotic frequency of the SSPP filter cell demonstrated a decreasing trend. This phenomenon can be attributed to the increase in the effective groove depth between the two limbs (i.e., the effective length of the branch) as the inclined branch rotates. As the angle θ increases, the effective length of the branch increases, leading to lower asymptotic frequencies in the SSPP filter cell.

As indicated in Eq. (1), the asymptotic frequency of the SSPP filter is closely related to the periodic distance d. It can be easily inferred that the asymptotic frequency is inversely proportional to d. This relationship is intuitively illustrated in Fig. 4. As the periodic distance d increases from 3.5 mm to 5.5 mm, the asymptotic frequency decreases from 11.1 GHz to 9.3 GHz.

2.2. Low-Pass Filter Structure Based on the SSPP Structure

The designed low-pass filter based on SSPP cell C with $\theta = 60°$ consists of three distinct sections, as shown in Fig. 5. Region I includes the input and output ports of the full filter, enabling the transmission of quasi-transverse electromagnetic (TEM) modes. To connect the input and output ports, the microstrip width was designed as $50\,\Omega$. Region II is a transition structure composed of the microstrip and two right-angled triangles on both sides of the microstrip. This region has two main purposes: to achieve impedance matching and convert the quasi-TEM modes to transverse magnetic (TM) modes, which can support the transmission of the SSPP mode surface wave.

Region III is the main region of the filter, where SSPP surface wave transmission occurs. This area is composed of six identical units arranged at the periodic distance d, as shown in Fig. 5. The blue portion represents the dielectric substrate (F4B) with a dielectric constant $\varepsilon_r = 2.65$, while the yellow portion represents the metal copper microstrip on the upper part of the substrate.

To verify the conclusions about the relationship between the cut-off frequency and the angle θ and periodic distance d presented in Section 2.1, several full SSPP filters with different values of θ and d were modelled, and the S-parameters of the structures were simulated.

As shown in Fig. 6(a), when d is 4.5 mm, the 3-dB cut-off frequencies at which θ equals $70°$, $60°$, and $50°$ are 9.5 GHz, 10.17 GHz, and 11.1 GHz, respectively. As θ decreases, the 3-dB cut-off frequency increases, while the out-of-band suppression within one octave is more than 20 dB. Fig. 6(b) shows that the filter has better standing waves for $\theta = 60°$.

Figure 7(a) shows curves of the S-parameters at different frequencies for various values of d. When $\theta = 60°$, the 3-dB cut-off frequencies are 11.25 GHz, 10.17 GHz, and 9.18 GHz for $d = 3.5$ mm, $d = 4.5$ mm, and $d = 5.5$ mm, respectively. As d increases, the 3-dB cut-off frequency decreases, accompanied by a slight deterioration in the out-of-band inhibition. The S_{11} parameter of the filter is shown in Fig. 7(b). The filter has the best passband standing waves when $d = 4.5$ mm.

Figure 8(a) illustrates the influence of the number of SSPP unit cells for $\theta = 60°$ and $d = 4.5$ mm. The curve of S_{21} moves to a lower frequency and decreases faster as the number of unit cells increases from 5 (corresponding to the red line) to 6 (corresponding to the green line). As the number of cells increases
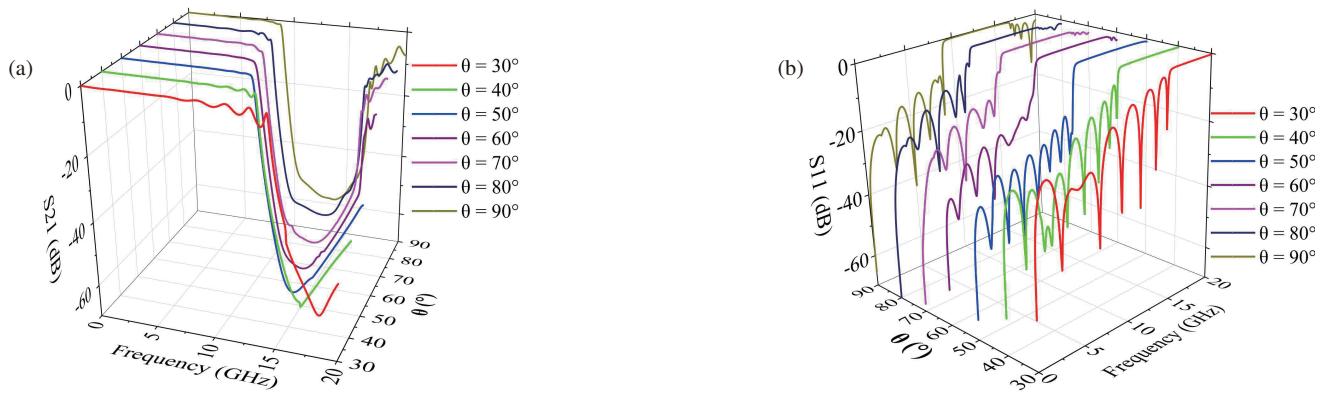
FIGURE 6. Simulated S-parameters (a) S_{21} and (b) S_{11} of the SSPP filter for various values of angle θ.
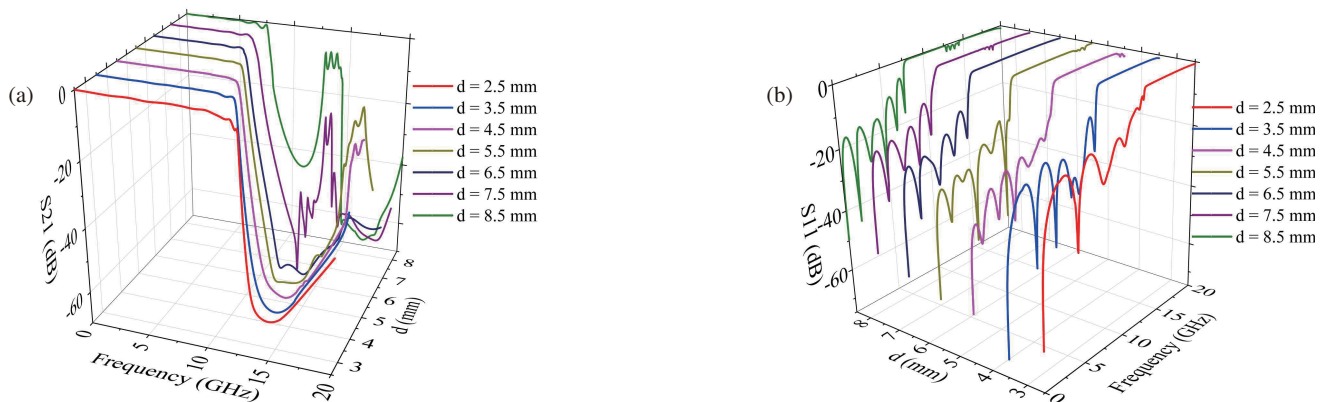
FIGURE 7. Simulated S-parameters (a) S_{21} and (b) S_{11} of the SSPP filter for various values of the periodic distance d.
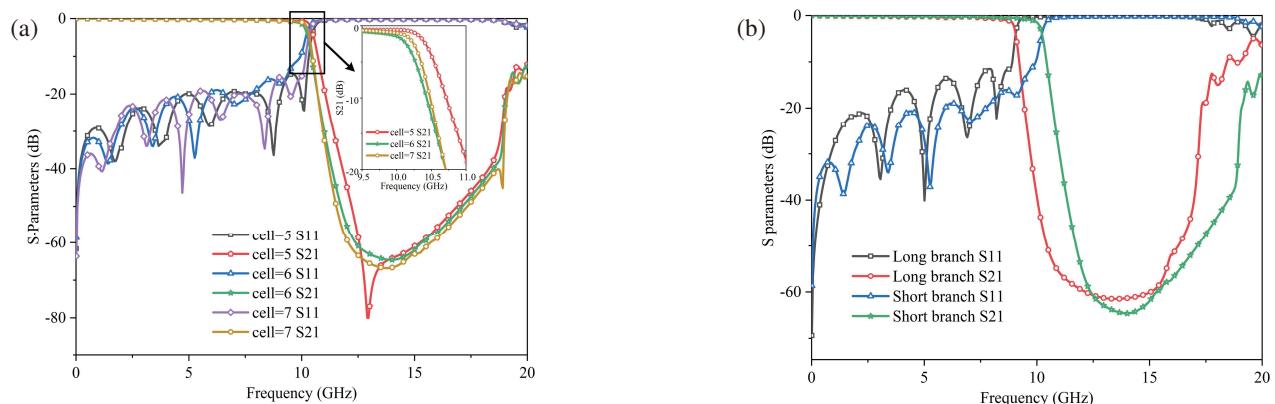
FIGURE 8. Simulated S-parameters of the SSPP filter for (a) various numbers of cells and (b) long branches and short branches.

from 6 to 7, the curve of S_{21} decreases slightly faster, but the change of curve of S_{21}, which is influenced by the number of cells, is not obvious, and the size increases. Considering the passband design index of the filter, therefore, 6-cell cells were chosen to design the SSPP filter.

To intuitively display the advantages of shorter branches over longer branches, two SSPP filters with the above two structures were designed, and their S-parameters were simulated. As shown in Fig. 8(b), the maximal S_{11} and the cut-off frequency of the filter using the long branch are -10 dB and 9.02 GHz,

while those of the filter using the short branch are -20 dB and 10.17 GHz, respectively. These results illustrate that using the short branch can decrease the S_{11} value of the filter. In addition, even if loading stepped shortened transverse branches leads to a slight increase in the asymptotic frequency, the groove depth $h1$ and width $(2h1 + w1)$ of the proposed SSPP filter are reduced by 26.22% and 24.84% compared with those of traditional SSPP structures, respectively. Moreover, due to the use of the new transition structure shown in Region II instead of the traditional transition structure with a gradual change in the
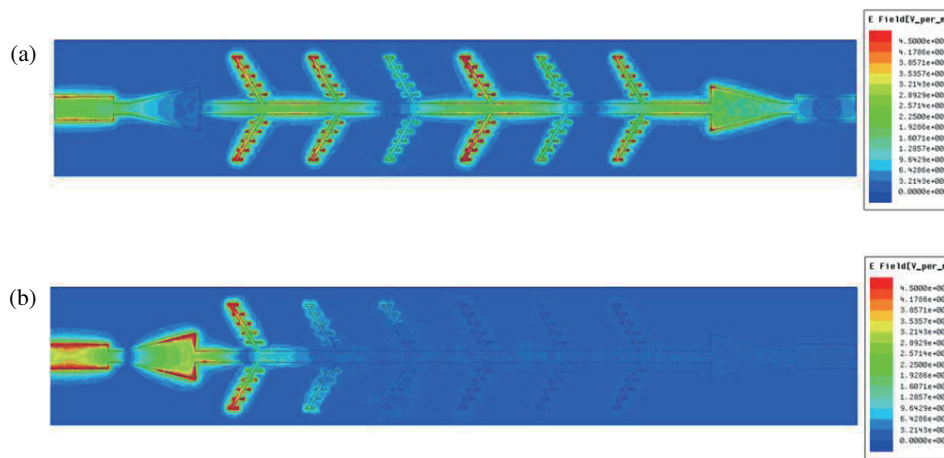
FIGURE 9. The simulated electric field distributions of the SSPP low-pass filter at (a) 6 GHz and (b) 12.5 GHz.
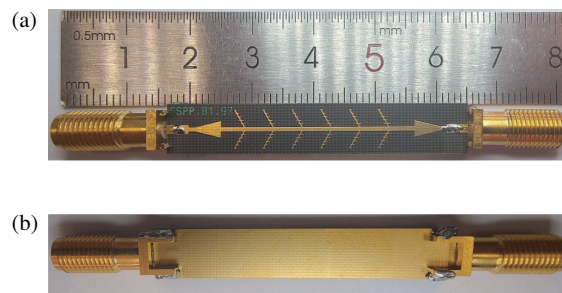
FIGURE 10. Photographs of the fabricated broadband low-pass filter: (a) top view and (b) botom view.

TABLE 1. Values of the main parameters.

Parameter	$\theta*$	$L1$	$L2$	$L3$	a	d	da
Value (mm)	$60°$	27	6.72	3.5	0.95	4.5	4.15
Parameter	h	$h1$	$h2$	ha	$l1$	$l2$	$l3$
Value (mm)	8	2.72	0.55	0.98	0.96	0.85	0.75
Parameter	$l4$	$l5$	la	$w1$	$w2$	$w3$	wa
Value (mm)	0.64	0.53	1.08	0.65	0.10	0.17	1.37

*θ is the angle formed between the inclined branch and the microstrip, so its unit is degrees

cell size, the length of the proposed SSPP filter decreases by 22.23%.

Figure 9 shows the simulated electric field distributions of the SSPP low-pass filter in the in-band and out-of-band regions. According to Fig. 9(a), the current can be input from the left port and pass through the full SSPP filter to the right port at 6 GHz in the in-band region. However, when the current is input from the left port, it cannot pass through the full SSPP filter at 12.5 GHz in the out-of-band region, as shown in Fig. 9(b).

3. MEASUREMENT RESULTS

To confirm the above simulation results, a low-pass filter based on the proposed SSPP structure was fabricated on a 0.5 mm thick F4B substrate ($\varepsilon_r = 2.65$, $\tan\delta = 0.001$, metal copper thickness is 0.035 mm). Its parameters and structure are the same as those shown in Table 1 and Fig. 5. Photographs of the

fabricated broadband low-pass filter are shown in Fig. 10, with Fig. 10(a) showing the top view and Fig. 10(b) showing the bottom view. The yellow layer is the copper, and the black layer is the F4B dielectric substrate. The cores of two SMA connectors are welded to the solder pads (Region I, shown in Fig. 5) at both ends of the filter, and the grounding pins of the connector are welded to the metal layer on the back of the filter. The size of the full structure is 47.44 mm×8 mm.

The 3672 series vector network analyzer (VNA) produced by Ceyear was used to measure the S-parameters of the filter. Fig. 11 shows the simulation and measurement results for the SSPP filter. The solid lines represent the measurement results, and the dashed lines represent the simulation results. The 3-dB cut-off frequency for the simulation results is 10.17 GHz, while that for the measurement results is 10.26 GHz, which is approximately 0.1 GHz higher than the cut-off frequency for
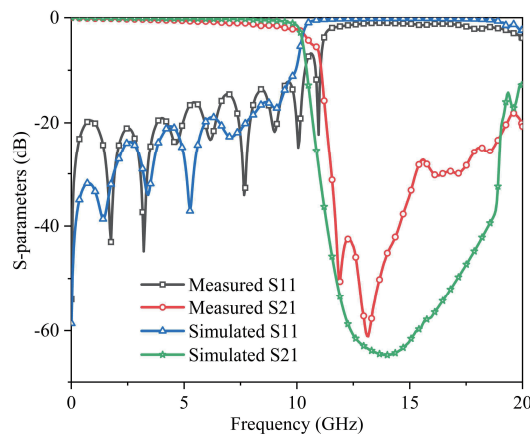
FIGURE 11. Measurement and simulation results of the S-parameters.
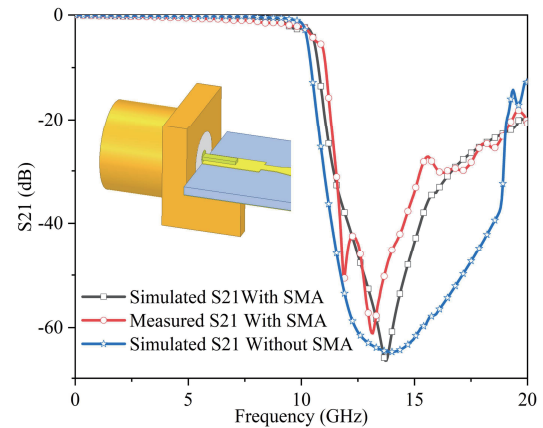
FIGURE 12. Measurement and simulation results with and without SMA connectors.
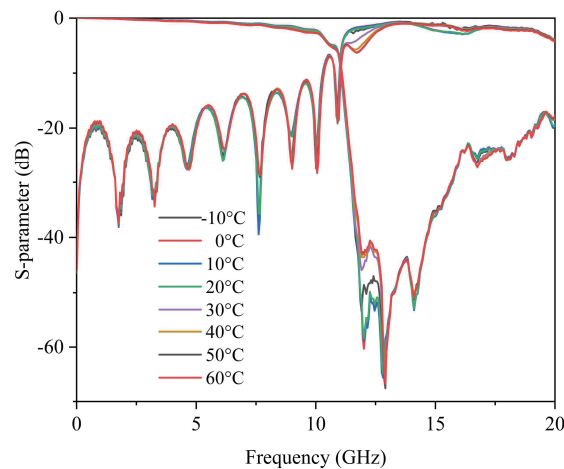
FIGURE 13. Measurement results of the S-parameters at different temperatures.

the simulation results. The 1-dB insertion loss bandwidths for simulation result and measurement results are 9.75 GHz and 7.01 GHz, respectively. The simulation and measurement insertion losses (ILs) are less than 3 dB from $0 \sim 10$ GHz. The simulation return loss (RL) is approximately more than 20 dB before 8 GHz, and the measurement RL is approximately more than 15 dB before 8 GHz and more than 12 dB between 8 GHz and 10 GHz. The measurement results slightly deviate from the simulation results. However, the full trend and 3-dB passband range of the measurement results are essentially consistent with the simulation results, which confirms the results presented in Section 2. Notably, the filter shows slightly poor selectivity in the high-frequency band. Previous reports have suggested that adding band-stop filters [33], resonators [34–36], varactor diodes, lumped elements [37], loading butterfly grooves [38], optimizing the mode conversion structure [39], and other methods can improve out-of-band suppression.

The biggest difference between the simulation and measurement results occurs in the out-of-band S_{21} parameters. The main reason is the production process, including the processing technology, fabrication errors, and SMA welding errors. SMA welding is the main cause of error. To verify the error

introduced by the two SMA connectors, the S_{21} parameter of proposed filter with them is simulated. As shown in Fig. 12, though the measurement result with SMA connectors has some difference from the simulation result without SMA connectors, it is basically the same as the simulation results with SMA connectors. The proposed filter is designed to use without SMA connectors.

To verify the stability of the filter at different temperatures, a series of temperature tests ranging from $-10°C$ to $60°C$ are done. Fig. 13 experiments the measurement results of the S-parameters. The S-parameter of the proposed filter shows only a slight variation with temperatures varying from $-10°C$ to $60°C$. The results indicate the nice temperature stability of the filter.

To highlight the advantages of the proposed compact SSPP low-pass filter, a Figure-Of-Merit (FOM) is proposed as a unified measure:

$$FOM = \frac{RL}{IL \times \frac{S}{\lambda_0^2}} \qquad (2)$$

where S represents the size of filter, and λ_0 represents the wavelength corresponding to the central operating frequency f_0. IL

TABLE 2. Comparison of the proposed filter and other SSPP filters.

Ref.	f_0/GHz	IL/dB	Min. RL/dB	Size/($\lambda_0 \times \lambda_0$)	FOM
[40]	5.7	4	8	2.66×0.46	1.63
[41]	4.1	4	6.5	1.84×0.26	3.39
[42]	6	5	6.5	2.44×0.2	2.66
[43]	4.45	3	8	1.56×0.17	10.06
[44]	2.25	2.5	7.5	1.38 0.17	13.2
[45]	2.42	3	8	0.75×0.1	35.56
This work	5.13	3	13	0.79×0.13	42.20

and RL indicate the insertion loss and minimum return loss in the passband of the SSPP filter, respectively. Higher FOM results represent better overall filter performance. Table 2 shows a comparison of the proposed SSPP filter and several other SSPP filters described in different references. Compared with the filters presented [40–45], the proposed compact SSPP low-pass filter has better performance in terms of size.

In future research, different materials such as plasma materials can be used to simulate and experiment the designed SSPP filter, and its performance can be compared to explore its more application values. Also, given that graphene [4] and Weyl semimetals TaAs and NbAs [9] have tunable properties, the proposed filter can also be integrated with graphene to achieve dynamic tuning referring to [46–48].

4. CONCLUSION

In this paper, a compact low-pass filter based on SSPP is proposed. The width and length of the filter were reduced by 24.84% and 22.23% by adopting a novel fishbone structure and a new transmission structure, respectively. The values of several key parameters of the proposed filter were simulated, and the asymptotic frequencies according to their dispersion curves were compared to determine the final parameter values for the SSPP cell. Then, the full structure of the SSPP filter was fabricated. The characteristics were simulated and experimentally measured. The measurement results show that the insertion loss and return loss are less than 3 dB and greater than 13 dB in a wideband range of 0–10.00 GHz, respectively. In addition, compared with other SSPP filters, the proposed SSPP filter has excellent performance in terms of size. The proposed filter can be used to compose microwave circuits, such as mixer, multiplier, and comb generator.

REFERENCES

[1] Barnes, W. L., A. Dereux, and T. W. Ebbesen, "Surface plasmon subwavelength optics," *Nature*, Vol. 424, No. 6950, 824–830, Aug. 2003.

[2] Politano, A., H. K. Yu, D. Farías, and G. Chiarello, "Multiple acoustic surface plasmons in graphene/Cu (111) contacts," *Physical Review B*, Vol. 97, No. 3, 035414, Jan. 2018.

[3] Politano, A., G. Chiarello, and C. Spinella, "Plasmon spectroscopy of graphene and other two-dimensional materials with transmission electron microscopy," *Materials Science in Semiconductor Processing*, Vol. 65, 88–99, Jul. 2017.

[4] Politano, A. and G. Chiarello, "Graphene on Pt3Ni(1 1 1): A suitable platform for tunable charge doping, electron–phonon coupling and plasmonic excitations," *2D Materials*, Vol. 4, No. 3, 035003, Jun. 2017.

[5] Politano, A., C. Lamuta, and G. Chiarello, "Cutting a gordian knot: Dispersion of plasmonic modes in Bi$_2$Se$_3$ topological insulator," *Applied Physics Letters*, Vol. 110, No. 21, 211601, May 2017.

[6] Politano, A., G. Chiarello, B. Ghosh, K. Sadhukhan, C.-N. Kuo, C. S. Lue, V. Pellegrini, and A. Agarwal, "3D dirac plasmons in the type-II Dirac semimetal PtTe2," *Physical Review Letters*, Vol. 121, No. 8, 086804, 2018.

[7] Dutta, D., B. Ghosh, B. Singh, H. Lin, A. Politano, A. Bansil, and A. Agarwal, "Collective plasmonic modes in the chiral multifold fermionic material CoSi," *Physical Review B*, Vol. 105, No. 16, 165104, Apr. 2022.

[8] Abramovich, S., D. Dutta, C. Rizza, S. Santoro, M. Aquino, A. Cupolillo, J. Occhiuzzi, M. F. L. Russa, B. Ghosh, D. Farias, A. Locatelli, D. W. Boukhvalov, A. Agarwal, E. Curcio, M. B. Sadan, and A. Politano, "NiSe and CoSe topological nodal-line semimetals: A sustainable platform for efficient thermoplasmonics and solar-driven photothermal membrane distillation," *Small*, Vol. 18, No. 31, 2201473, Aug. 2022.

[9] Chiarello, G., J. Hofmann, Z. Li, V. Fabio, L. Guo, X. Chen, S. D. Sarma, and A. Politano, "Tunable surface plasmons in weyl semimetals TaAs and NbAs," *Physical Review B*, Vol. 99, No. 12, 121401, Mar. 2019.

[10] Politano, A., L. Viti, and M. S. Vitiello, "Optoelectronic devices, plasmonics, and photonics with topological insulators," *APL Materials*, Vol. 5, No. 3, 035504, Mar. 2017.

[11] Liang, F., L. Zhan, T. Guo, X. Wu, and J. Chu, "CVD-Grown 2D nonlayered NiSe as a broadband photodetector," *Micromachines*, Vol. 12, No. 9, 1066, Sep. 2021.

[12] Politano, A., G. Chiarello, Z. Li, V. Fabio, L. Wang, L. Guo, X. Chen, and D. W. Boukhvalov, "Toward the effective exploitation of topological phases of matter in catalysis: Chemical reactions at the surfaces of NbAs and TaAs Weyl semimetals," *Advanced Functional Materials*, Vol. 28, No. 23, 1800511, Jun. 2018.

[13] Pan, L., Y. Wu, and W. Wang, "Bandpass filter with reconfigurable rejection and deep-upper-wideband harmonics suppres-

sion using spoof surface plasmon polaritons of hollowed-bow-tie cells," *IEEE Transactions on Microwave Theory and Techniques*, Vol. 71, No. 4, 1–9, 2023.

[14] Zhu, S., P. Wen, and Y. Liu, "A compact filter based on spoof surface plasmon polariton waveguide for wide stopband suppression," *IEEE Photonics Technology Letters*, Vol. 34, No. 9, 475–478, May 2022.

[15] Lin, Z., Y. Li, L. Li, Y.-T. Zhao, J. Xu, and J. Chen, "Miniaturized bandpass filter based on high-order mode of spoof surface plasmon polaritons loaded with capacitor," *IEEE Transactions on Plasma Science*, Vol. 51, No. 1, 254–260, Jan. 2023.

[16] Li, J., J. Shi, K.-D. Xu, Y.-J. Guo, A. Zhang, and Q. Chen, "Spoof surface plasmon polaritons developed from coplanar waveguides in microwave frequencies," *IEEE Photonics Technology Letters*, Vol. 32, No. 22, 1431–1434, Nov. 2020.

[17] Li, J., K.-D. Xu, J. Shi, Y.-J. Guo, and A. Zhang, "Spoof surface plasmon polariton waveguide with switchable notched band," *IEEE Photonics Technology Letters*, Vol. 33, No. 20, 1147–1150, Oct. 2021.

[18] Feng, W., Y. Feng, Y. Shi, S. Shi, and W. Che, "Novel differential bandpass filter using spoof surface plasmon polaritons," *IEEE Transactions on Plasma Science*, Vol. 48, No. 6, 2083–2088, Jun. 2020.

[19] Zhang, D., K. Zhang, Q. Wu, X. Ding, and X. Sha, "High-efficiency surface plasmonic polariton waveguides with enhanced low-frequency performance in microwave frequencies," *Optics Express*, Vol. 25, No. 3, 2121–2129, 2017.

[20] Zhang, D., K. Zhang, Q. Wu, R. Dai, and X. Sha, "Broadband high-order mode of spoof surface plasmon polaritons supported by compact complementary structure with high efficiency," *Optics Letters*, Vol. 43, No. 13, 3176–3179, 2018.

[21] Kianinejad, A., Z. N. Chen, and C.-W. Qiu, "Design and modeling of spoof surface plasmon modes-based microwave slow-wave transmission line," *IEEE Transactions on Microwave Theory and Techniques*, Vol. 63, No. 6, 1817–1825, Jun. 2015.

[22] Pendry, J. B., L. Martín-Moreno, and F. J. Garcia-Vidal, "Mimicking surface plasmons with structured surfaces," *Science*, Vol. 305, No. 5685, 847–848, Aug. 2004.

[23] Garcia-Vidal, F. J., L. Martín-Moreno, and J. B. Pendry, "Surfaces with holes in them: New plasmonic metamaterials," *Journal of Optics A: Pure and Applied Optics*, Vol. 7, No. 2, S97–S101, Feb. 2005.

[24] O'Hara, J. F., R. D. Averitt, and A. J. Taylor, "Terahertz surface plasmon polariton coupling on metallic grating structures," in *Ultrafast Phenomena XIV*, Vol. 79, 696–698, Niigata, Japan, Jul. 2005.

[25] Williams, C. R., S. R. Andrews, S. A. Maier, A. I. Fernández-Domínguez, L. Martín-Moreno, and F. J. García-Vidal, "Highly confined guiding of terahertz surface plasmon polaritons on structured metal surfaces," *Nature Photonics*, Vol. 2, No. 3, 175–179, Mar. 2008.

[26] Zhang, D., K. Zhang, Q. Wu, G. Yang, and X. Sha, "High-efficiency broadband excitation and propagation of second-mode spoof surface plasmon polaritons by a complementary structure," *Optics Letters*, Vol. 42, No. 14, 2766–2769, Jul. 2017.

[27] Li, L., L. Dong, P. Chen, and K. Yang, "A low insertion loss low-pass filter based on single comb-shaped spoof surface plasmon polaritons," *International Journal of Microwave and Wireless Technologies*, Vol. 11, No. 8, 792–796, Oct. 2019.

[28] Zhang, X., S. Sun, Q. Yu, L. Wang, K. Liao, and S. Liu, "Novel high-efficiency and ultra-compact low-pass filter using double-layered spoof surface plasmon polaritons," *Microwave and Optical Technology Letters*, Vol. 64, No. 6, 1056–1061, Jun. 2022.

[29] Liu, L., Z. Li, B. Xu, J. Xu, C. Chen, and C. Gu, "Fishbone-like high-efficiency low-pass plasmonic filter based on double-layered conformal surface plasmons," *Plasmonics*, Vol. 12, No. 2, 439–444, Apr. 2017.

[30] Ma, H. F., X. Shen, Q. Cheng, W. X. Jiang, and T. J. Cui, "Broadband and high-efficiency conversion from guided waves to spoof surface plasmon polaritons," *Laser & Photonics Reviews*, Vol. 8, No. 1, 146–151, Jan. 2014.

[31] Shen, X., T. J. Cui, D. Martin-Cano, and F. J. Garcia-Vidal, "Conformal surface plasmons propagating on ultrathin and flexible films," *Proceedings of the National Academy of Sciences*, Vol. 110, No. 1, 40–45, Jan. 2013.

[32] Nagpal, P., N. C. Lindquist, S.-H. Oh, and D. J. Norris, "Ultrasmooth patterned metals for plasmonics and metamaterials," *Science*, Vol. 325, No. 5940, 594–597, Jul. 2009.

[33] Chen, Y., Z. Song, Y. Li, M. Hu, Q. Xing, Z. Zhang, L. Chai, and C.-Y. Wang, "Effective surface plasmon polaritons on the metal wire with arrays of subwavelength grooves," *Optics Express*, Vol. 14, No. 26, 13 021–13 029, 2006.

[34] Maier, S. A., S. R. Andrews, L. Martín-Moreno, and F. J. García-Vidal, "Terahertz surface plasmon-polariton propagation and focusing on periodically corrugated metal wires," *Physical Review Letters*, Vol. 97, No. 17, 176805, Oct. 2006.

[35] Hibbins, A. P., B. R. Evans, and J. R. Sambles, "Experimental verification of designer surface plasmons," *Science*, Vol. 308, No. 5722, 670–672, Apr. 2005.

[36] Moreno, E., S. G. Rodrigo, S. I. Bozhevolnyi, L. Martín-Moreno, and F. J. García-Vidal, "Guiding and focusing of electromagnetic fields with wedge plasmon polaritons," *Physical Review Letters*, Vol. 100, No. 2, 023901, Jan. 2008.

[37] Gan, Q., Z. Fu, Y. J. Ding, and F. J. Bartoli, "Ultrawide-bandwidth slow-light system based on thz plasmonic graded metallic grating structures," *Physical Review Letters*, Vol. 100, No. 25, 256803, Jun. 2008.

[38] Kianinejad, A., Z. N. Chen, and C.-W. Qiu, "Low-loss spoof surface plasmon slow-wave transmission lines with compact transition and high isolation," *IEEE Transactions on Microwave Theory and Techniques*, Vol. 64, No. 10, 3078–3086, Oct. 2016.

[39] Shen, X. and T. J. Cui, "Planar plasmonic metamaterial on a thin film with nearly zero thickness," *Applied Physics Letters*, Vol. 102, No. 21, 211909, May 2013.

[40] Xu, K.-D., H. Xu, and Y. Liu, "Low-profile filtering end-fire antenna integrated with compact bandstop filtering element for high selectivity," *IEEE Access*, Vol. 7, 8398–8403, 2019.

[41] Farokhipour, E., M. Mehrabi, N. Komjani, and C. Ding, "A spoof surface plasmon polaritons (SSPPs) based dual-band-rejection filter with wide rejection bandwidth," *Sensors*, Vol. 20, No. 24, 7311, Dec. 2020.

[42] Mazdouri, B., M. M. Honari, and R. Mirzavand, "Miniaturized spoof SPPs filter based on multiple resonators or 5G applications," *Scientific Reports*, Vol. 11, No. 1, 22557, Nov. 2021.

[43] Moznebi, A.-R., K. Afrooz, and A. Arsanjani, "Broadband bandpass filter and filtering power divider with enhanced slow-wave effect, compact size, and wide stopband based on butterfly-shaped spoof spps," *AEU-International Journal of Electronics and Communications*, Vol. 145, 154084, Feb. 2022.

[44] Cui, Y., K.-D. Xu, and Q. Chen, "Bandpass filter using half-mode substrate integrated plasmonic waveguide," in *2020 IEEE Asia-Pacific Microwave Conference (APMC)*, 29–30, Hong Kong, Dec. 2020.

[45] Fernandez-Dominguez, A. I., L. Martin-Moreno, F. J. Garcia-Vidal, S. R. Andrews, and S. A. Maier, "Spoof surface plasmon polariton modes propagating along periodically corrugated

wires," *IEEE Journal of Selected Topics in Quantum Electronics*, Vol. 14, No. 6, 1515–1521, Nov.-Dec. 2008.

[46] Wu, B., C. Fan, X. Feng, Y.-T. Zhao, J. Ning, D. Wang, and T. Su, "Dynamically tunable filtering attenuator based on graphene integrated microstrip resonators," *IEEE Transactions on Microwave Theory and Techniques*, Vol. 68, No. 12, 5270–5278, Dec. 2020.

[47] Yi, Y. and A.-Q. Zhang, "A tunable graphene filtering attenuator based on effective spoof surface plasmon polariton waveg-

uide," *IEEE Transactions on Microwave Theory and Techniques*, Vol. 68, No. 12, 5169–5177, Dec. 2020.

[48] Tian, D., A. Kianinejad, A. Zhang, and Z. N. Chen, "Graphene-based dynamically tunable attenuator on spoof surface plasmon polaritons waveguide," *IEEE Microwave and Wireless Components Letters*, Vol. 29, No. 6, 388–390, Jun. 2019.